A HERSCHEL LOOK TO STAR FORMATION IN THE THIRD GALACTIC QUADRANT

D. Elia[1], S. Molinari[1], Y. Fukui[2], E. Schisano[1,3], L. Olmi[4,5], M. Veneziani[3], T. Hayakawa[2], M. Pestalozzi[1], N. Schneider[6], M. Benedettini[1], A. M. di Giorgio[1], D. Ikhenaode[7], A. Mizuno[8], T. Onishi[9], S. Pezzuto[1], L. Piazzo[6], D. Polychroni[10], K. L. J. Rygl[1], H. Yamamoto[2], Y. Maruccia[11]

1. Istituto di Astrofisica e Planetologia Spaziali - INAF, Roma, Italy, davide.elia@iaps.inaf.it. 2. Department of Physics, Nagoya University, Japan. 3. Infrared Processing and Analysis Center, California Institute of Technology, Pasadena, CA, USA. 4. Osservatorio Astrofisico di Arcetri - INAF, Firenze, Italy. 5. University of Puerto Rico, Physics Department, San Juan, PR, USA. 6. IRFU/SAp CEA/DSM, Laboratoire AIM CNRS, Université Paris Diderot, Gif-sur-Yvette, France. 7. Dipartimento di Ingegneria dell'Informazione, Elettronica e Telecomunicazioni, Università di Roma La Sapienza, Roma, Italy. 8. Solar-Terrestrial Environment Laboratory, Nagoya University, Japan. 9. Department of Physical Science, Osaka Prefecture University, Japan. 10. Department of Astrophysics, Astronomy and Mechanics, Faculty of Physics, University of Athens, Greece. 11. Dipartimento di Matematica e Fisica, Università del Salento, Lecce, Italy.

Published (2013) on ApJ, 772, 45

ABSTRACT

The first Hi-GAL observations of the outer Galaxy consist of five dust continuum maps, between 70 and 500 μm, of the area delimited by 216.5° ≤ ℓ ≤ 225.5° and −2° ≤ b ≤ 0°). NANTEN CO(1-0) line observations are used to derive cloud kinematics and distances, making it possible to estimate physical parameters of the compact sources (cores and clumps) detected in the region, namely 255 proto-stellar and 590 pre-stellar sources, respectively. Both source typologies are found in all the distance components observed in the field, up to ~6 kpc, testifying the presence of star formation beyond the Perseus arm at these longitudes. Furthermore, several sources of both proto- and pre-stellar nature are compatible with requirements for massive star formation, based on the mass-radius relation. For the pre-stellar sources belonging to the Local arm (d ≤ 1.5 kpc) we study the mass function, whose high-mass end shows a power-law behavior $N(\log M) \propto M^{-1.2\pm0.2}$. Finally, we use a luminosity versus mass diagram to infer the evolutionary status of the sources, finding that most of the proto-stellar are in the early accretion phase (with some cases compatible with a Class I stage), while for pre-stellar sources, in general, accretion has not started yet.

OBSERVATIONS AND DATA REDUCTION

Here we show a study based on the first four "tiles" observed in the Third Galactic Quadrant (TGQ) as part of the Herschel Infrared Galactic plane survey (Hi-GAL; Molinari et al. 2010, PASP, 122, 314). They span the ranges 216.5° ≤ ℓ ≤ 225.5° and −2° ≤ b ≤ 0° (hereafter, we will call *ℓ217–224* the entire region). The maps were obtained using simultaneously PACS at 70 and 160 μm and SPIRE at 250, 350, and 500 μm. The the area covered by both PACS and SPIRE amounts to ~20.5 deg^2.

The NANTEN CO(1–0) Galactic Plane Survey data set (Mizuno & Fukui 2004, ASP Conf. Ser., 317, 59) was also used to reconstruct the gas kinematics in this area.

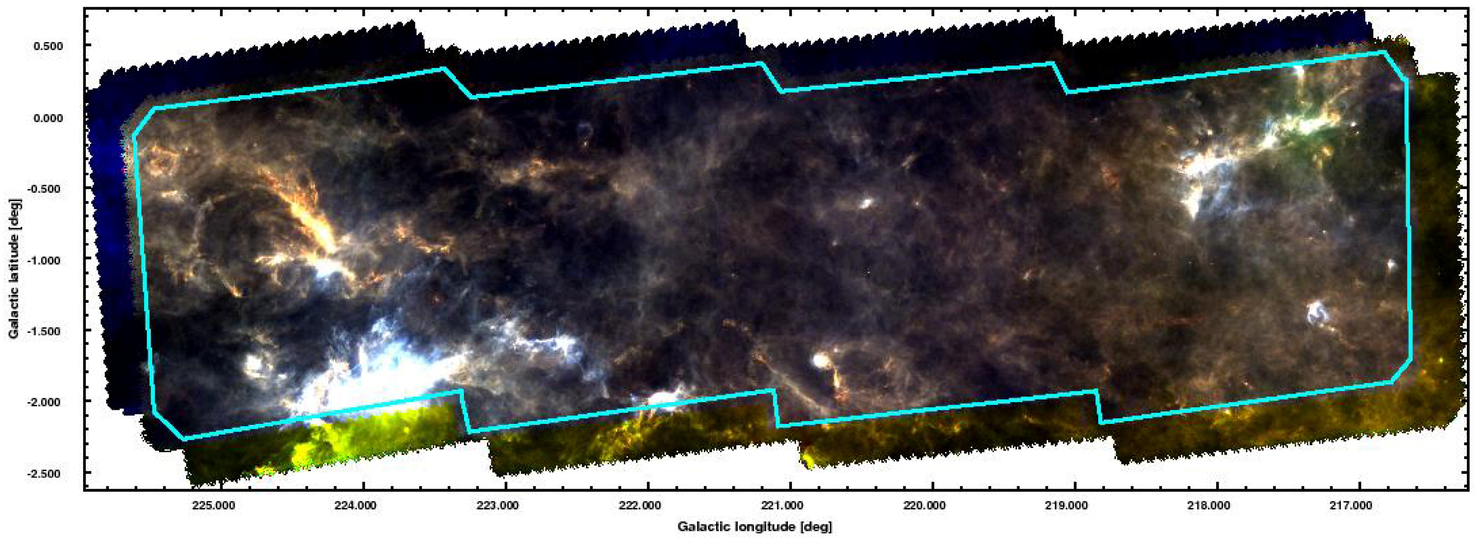

FIGURE 1. RGB composite of *ℓ217–224* (blue: PACS 160μm; green: SPIRE 250μm; red: SPIRE 500 μm). The color scaling is linear. The cyan contour delimits the common science area covered by both PACS and SPIRE.

VELOCITY FIELD

Three main components are found, peaking at 17, 28, 40, and 54 km s^{-1} , respectively (Figure 2). They correspond to four main distance components located around heliocentric distances of 1.1, 2.2, 3.3, and 5.8 kpc, respectively. In Figure 3 we highlight the low degree of complexity of the velocity field: the eastern part of the region is dominated by the first (bluest) component, the western one is dominated by the second component, whereas the third and fourth components are associated with few smaller features of the SPIRE map.

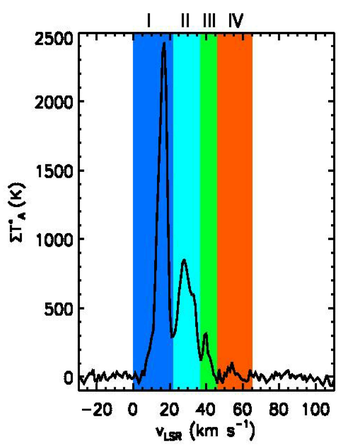

FIGURE 2. Sum of all the CO(1–0) spectra in the *ℓ217–224* region. The four velocity ranges delimited by −0.5, 20.5, 36.5, 44.5, and 65.5 km s^{-1} are considered as different distance components, labeled with numerals I, II, III, and IV and highlighted with a blue, cyan, green, and red background, respectively.

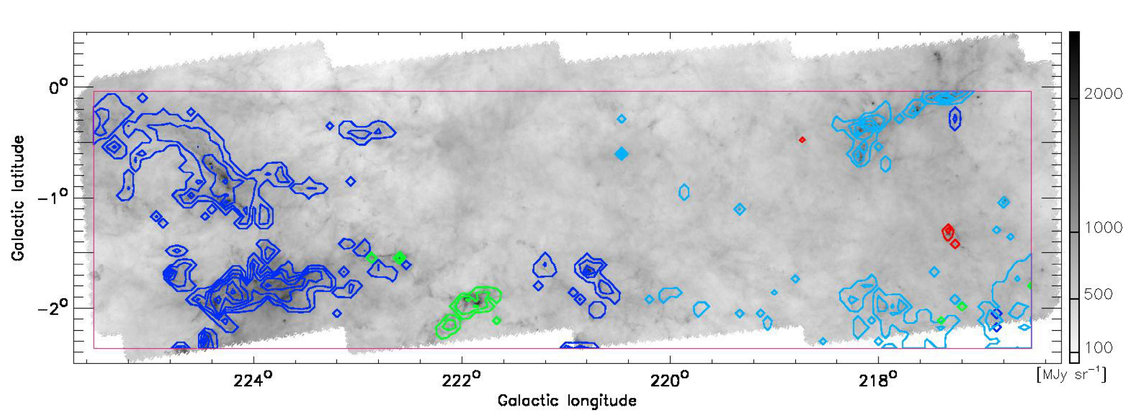

FIGURE 3. Contours of integrated intensity of the four CO(1-0) components, overplotted on the SPIRE 250μm map, with the same color convention of Figure 2. The magenta box delimits the area surveyed in the CO(1–0).

COMPACT SOURCES

Compact sources have been extracted at each of the five Hi-GAL bands using CuTEx (Molinari et al. 2011, A&A, 530, A133). After band-merging for obtaining a five-band catalog, 943 sources eligible for grey-body fit (i.e. with a regular SED and a distance estimate obtained through spatial association with the CO emission) have been selected (Figure 4). Ancillary WISE photometry has been also exploited, so that finally 255 protostellar sources (i.e. provided with a 70 μm and/or a 22+160 μm detection) and 688 starless ones have been identified. Figures 5 shows the displacement of these sources in the Galactic plane, while Figures 6 and 7 present the statistics of some basic physical properties of them.

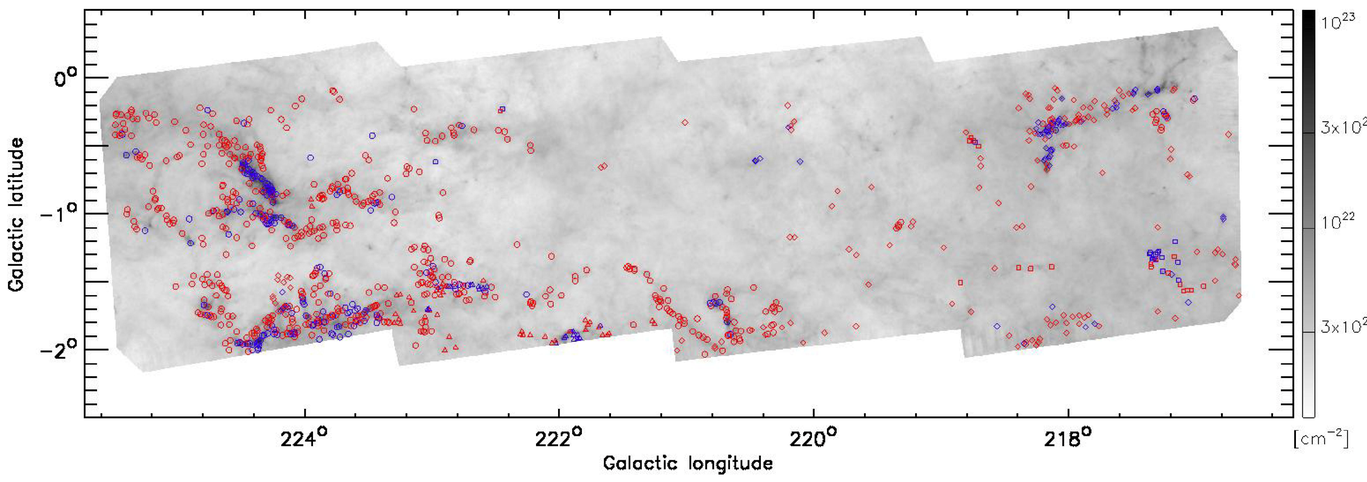

FIGURE 4. Hi-GAL compact sources positions overplotted on the column density map. Circles, triangles, diamonds, and squares correspond to the distance components I, II, III, and IV, respectively. The blue and red colors indicate protostellar and starless sources, respectively.

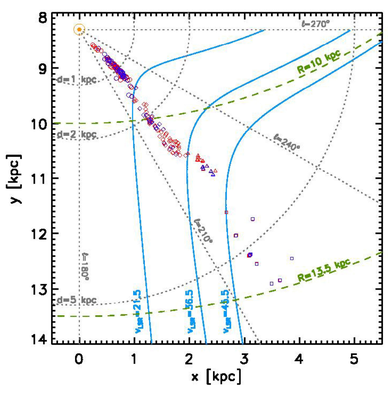

FIGURE 5. Galactic positions of the compact sources in *ℓ217–224*. The origin of the axes is in the Galactic center. The symbol and color conventions are the same as in Figure 4. The orange symbol represents the position of the Sun. The cyan solid lines are isotachs corresponding to the three V_{lsr} values separating the four main CO(1–0) components we identified.

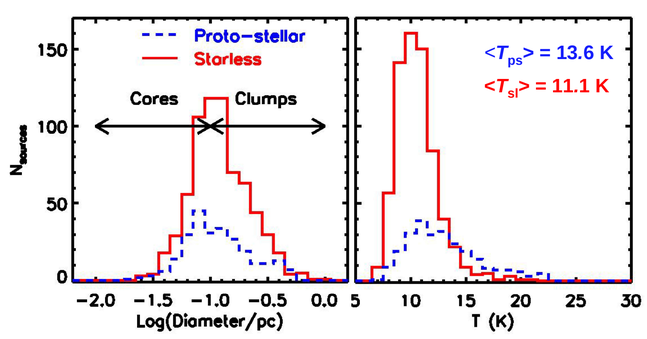

FIGURE 6. Histograms of diameter (left) and temperature (right) of starless (red) and proto-stellar (blue) sources. Notice that our sample is composed by a mixture of clumps and cores, and that, on average, the proto-stellar sources are slightly warmer that the pre-stellar ones.

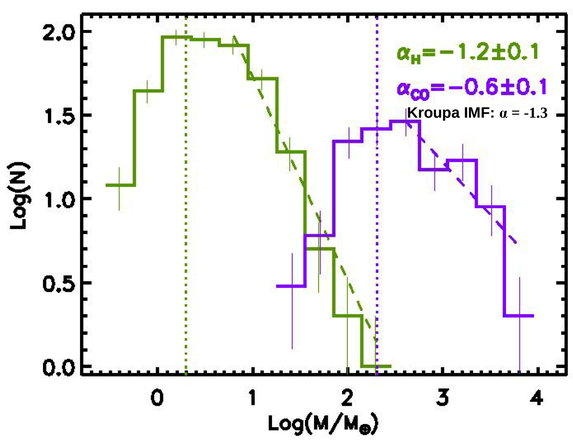

FIGURE 7. Source mass distribution for the component I (green: Hi-GAL pre-stellar sources; purple: CO clumps extracted running CLUMPFIND). The slopes of the power-law fit to the linear portion of the two distributions (dashed lines) are reported. The dotted vertical lines represent the mass completeness limits. The discrepancy between the two slopes is a consequence of the different resolution: NANTEN sources are resolved by Herschel, revealing a certain degree of fragmentation.

STABILITY, EVOLUTION

The mass versus radius plot (Figure 8) is helpful to study the gravitational stability of the starless cores. Starless sources with a mass exceeding the their Bonnor-Ebert mass ($M_{BE}[M_\odot]$ = 2.4/G R[pc] c_s[m s^{-1}]) are considered gravitationally bound, then pre-stellar. Moreover, by comparison with thresholds for massive star formation several *ℓ217–224* sources (belonging to all the four components) are found to be candidates to form massive stars.

The plot of bolometric luminosity vs the envelope mass (Figure 9), instead, is used (e.g. Molinari et al. 2008, A&A, 481, 345) to infer the source evolutionary status through the comparison with theoretical tracks obtained from models of accreting cores. Such tracks initially follow an almost vertical path corresponding to the accretion phase. Subsequently, the proto-stellar outflow activity produces mass loss and disperses the residual envelope (horizontal portion of the tracks). We find a significant segregation between pre- and proto-stellar sources in this diagram: the latter populate a region corresponding to ongoing accretion, while the former lie in a region corresponding to a earlier stage. Furthermore, the most evolved sources are, in general, also the warmest.

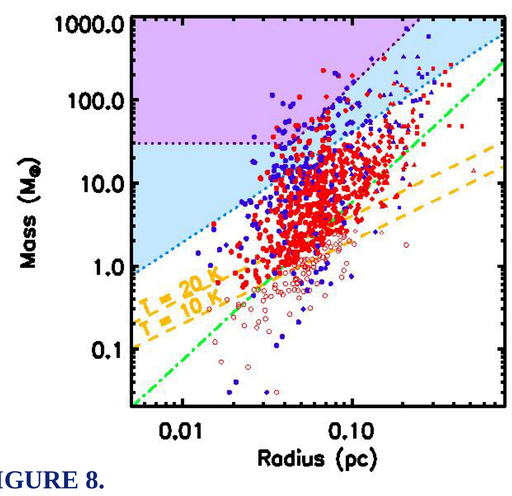

FIGURE 8. Mass vs. radius diagram for the Hi-GAL sources in *ℓ217–224*. Symbols, with the same shape convention of Figure 5, represent starless unbound (red open), pre-stellar (red filled) and proto-stellar (blue filled) sources. Orange dashed lines are the loci of the Bonnor-Ebert for T = 10 K and 20 K, while the green dot-dashed line represents the Larson (1981, MNRAS, 194, 809) third law. The purple and a blue background areas are the regions corresponding to the conditions for massive star formation to occur, according to the Krumholz & McKee (2008, Nature, 451, 1082) and Kauffmann & Pillai (2010, ApJL, 723, L7) thresholds for massive star formation.

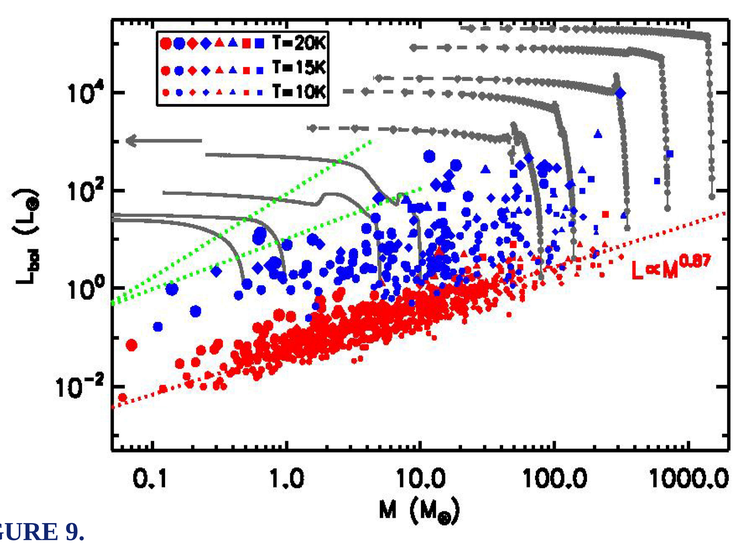

FIGURE 9. Bolometric luminosity vs. the mass of the same sources of Figure 8. Here the symbol size varies according to the source temperature. Gray and black solid lines represent the evolutionary tracks for the low- and high-mass regimes, respectively (Molinari et al., 2008). The gray arrow indicates the evolution direction, while dashed green lines delimit the region of transition between Class 0 and Class I sources (André et al. 2000, PPIV, 59) in the low-mass regime. The red dotted line represents the best-fitting power law ($L_{bol} \propto M_{env}^{0.87\pm0.02}$) for the distribution of the pre-stellar sources.